Missing-level statistics in a dissipative microwave resonator with partially violated time-reversal invariance

Małgorzata Białous [1], Barbara Dietz [2,*], and Leszek Sirko [1,†]

[1]*Institute of Physics, Polish Academy of Sciences, Aleja Lotników 32/46, 02-668 Warszawa, Poland*
[2]*Lanzhou Center for Theoretical Physics and the Gansu Provincial Key Laboratory of Theoretical Physics,*
Lanzhou University, Lanzhou, Gansu 730000, China

We report on the experimental investigation of the fluctuation properties in the resonance frequency spectra of a flat resonator simulating a dissipative quantum billiard subject to partial time-reversal-invariance violation (TIV) which is induced by two magnetized ferrites. The cavity has the shape of a quarter bowtie billiard of which the corresponding classical dynamics is chaotic. Due to dissipation it is impossible to identify a complete list of resonance frequencies. Based on a random-matrix theory approach we derive analytical expressions for statistical measures of short- and long-range correlations in such incomplete spectra interpolating between the cases of preserved time-reversal invariance and complete TIV and demonstrate their applicability to the experimental spectra.

I. INTRODUCTION

The conjecture [1–3] that the fluctuation properties in the eigenvalue spectra of typical quantum systems with fully chaotic classical limit coincide with those of random matrices from the Gaussian ensembles [4] has become the cornerstone of many theoretical, experimental, and numerical studies in the field of quantum chaos. The spectral properties of generic quantum systems with fully chaotic classical dynamics and preserved time-reversal ($\mathcal{T}$) invariance coincide with those of random matrices from the Gaussian orthogonal ensemble (GOE). Some examples are quantum wells [5], molecular spectra [6], atoms in a strong microwave field [7,8], flat microwave resonators (billiards) [9–15], and microwave networks [16–19]. In the presence of $\mathcal{T}$-invariance violation (TIV) the spectral properties are well described by those of random matrices from the Gaussian unitary ensemble (GUE). This was observed, for example, for atoms in a constant external magnetic field [20], graphene quantum dots [21], Rydberg excitons [22], nuclear reactions [23,24], microwave billiards [25–27], and networks [28–34]. A random-matrix theory (RMT) approach was also developed for quantum systems with partially violated $\mathcal{T}$ invariance [35–38]. Such systems were realized experimentally by inserting ferritic material into a microwave billiard and magnetizing it with an external magnetic field [25–27,39]. The degree of time irreversibility can be adjusted by controlling the magnitude of the applied magnetic field and quantified by a parameter which interpolates between the cases of a $\mathcal{T}$-invariant system and a system with complete TIV [33,35,37,40,41]. We would like to mention that dissipative microwave billiards subject to partial TIV were previously used in a different context in

Refs. [42,43] to investigate the features of dissipative quantum systems with partial TIV in the vicinity of exceptional points, that is, those of isolated pairs of nearly degenerate resonance frequencies. Furthermore, the fluctuation properties in the level sequence of a flat microwave resonator or quantum billiard are determined by their shape. Therefore, billiards are often used for the numerical, theoretical, and experimental investigation of the features of quantum chaos.

Generally, the completeness of a spectrum is indispensable for the comparison of the fluctuation properties with those of random matrices from the Gaussian ensembles. However, complete sequences of several hundreds of levels are achievable only very rarely. One example are high-precision measurements of resonance spectra performed with flat, superconducting resonators at liquid-helium temperature [15,40,44,45] yielding sharp and well isolated resonances, and thus making the determination of the resonance frequencies from the positions of the resonances feasible. Due to absorption, measurements at room temperature typically yield overlapping resonances, which render the determination of complete sequences of resonances impossible. Thus, experimentally determined level sequences are typically incomplete and lead to deviations of the spectral properties from RMT predictions for complete spectra. To overcome these difficulties one has to cope with missing levels, which has been made feasible with the RMT approach for missing levels introduced in Ref. [46]. It was developed in the context of nuclear physics in Refs. [46–49] and applied to atomic, molecular, and nuclear systems [6,50–56] and to microwave billiards and microwave networks [29,57,58] simulating quantum billiards and graphs with preserved $\mathcal{T}$ invariance and complete TIV.

The objective of this article is to analyze the spectral fluctuations in the resonance frequency spectra of a real system, a microwave resonator with internal absorption which leads to the incompleteness of the spectra, in the presence of partial TIV. We present analytical results accounting for partial TIV
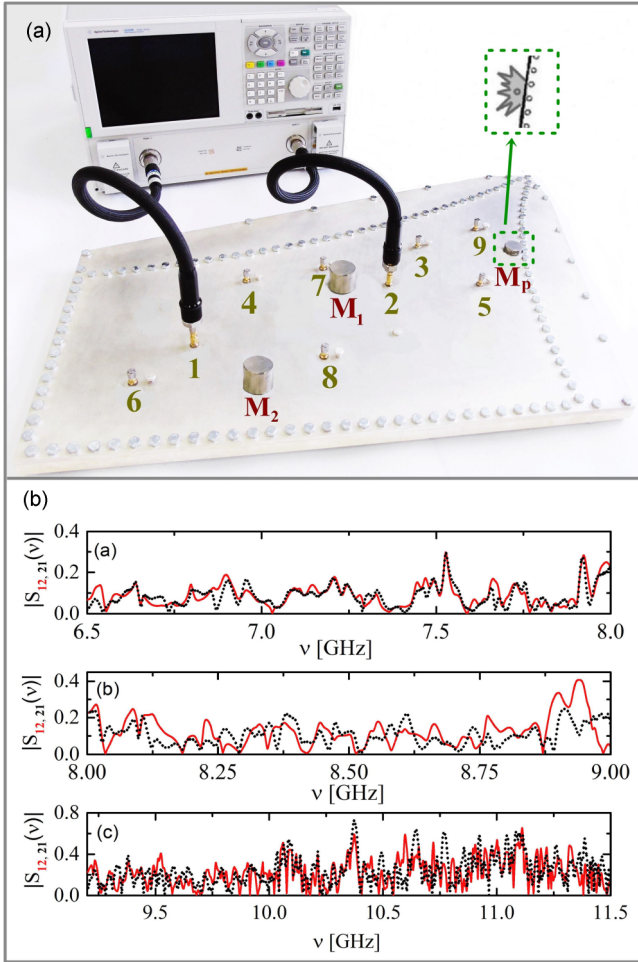
*Dietz@lzu.edu.cn
†sirko@ifpan.edu.pl

FIG. 1. (a) The experimental setup. The vector network analyzer Agilent E8364B is connected to the microwave antennas, which are attached to the resonator through the flexible microwave cables. In order to induce $\mathcal{T}$-invariance violation two pieces of ferrite are inserted into the cavity and magnetized by four external magnets placed at the positions of the ferrites below and above the resonator. The latter are marked by M_1 and M_2. An additional magnet M_P is used to move a metallic perturber inside the cavity alongside its walls to create different realizations of the cavity. (b) Transmission spectra from antenna 1 to antenna 2 (black dotted line) and vice versa (red full line) in three frequency regions.

in terms of a parameter ξ [37] which interpolates between GOE and GUE and for the incompleteness of the level sequence which is characterized by the fraction Φ of identified levels. In Sec. II we describe the experimental setup and then introduce in Sec. III the RMT approach for missing levels and apply it to the experimental level sequences. In Sec. IV we summarize the results.

II. EXPERIMENTAL SETUP

We used the same microwave cavity [see Fig. 1(a)] as in our previous work on the enhancement factor as function of openness and size of TIV [41,59]. It has the shape of a quarter bowtie billiard of which the classical dynamics is fully chaotic. The cavity consists of two plates of polished

aluminum type EN 5754. A basin of area $\mathcal{A} = 1828.5 \pm 5.0$ cm^2, perimeter $\mathcal{L} = 202.3 \pm 2.0$ cm, and depth $h = 1.2$ cm, which forms the resonator body, was milled out of the bottom plate. The inner surface of the cavity is covered with a 20-μm layer of silver to reduce internal absorption. Below the cutoff frequency of $\nu_{\max} = c/2h \simeq 12.49$ GHz, with c denoting the speed of light in vacuum, only the transverse magnetic modes are excited inside the cavity so that the Helmholtz equation describing the electromagnetic field in the microwave cavity and the two-dimensional Schrödinger equation for the quantum billiard of corresponding shape are mathematically equivalent. The top plate of the cavity has nine identical, randomly distributed holes marked from 1 to 9 in Fig. 1. In our previous experiments these holes were shunted with 50 Ω loads to realize up to nine scattering channels. For the analysis of the fluctuation properties of the resonance frequencies we consider only $M = 2$ scattering channels since, as was shown in Ref. [41], for this case TIV is strongest in a given frequency interval. Furthermore, for increasing openness and internal absorption the overlap of the resonances becomes stronger and renders the identification of the resonance frequencies impossible.

In order to measure the two-port scattering matrix $\hat{S}(\nu)$ two antennas of lengths 5.8 mm and pin diameter 0.9 mm were attached to the microwave cavity at the positions marked by 1 and 2 in Fig. 1(a) and connected to an Agilent E8364B vector network analyzer (VNA). The two antennas correspond to the $M = 2$ scattering channels. A metallic perturber with perimeter ≈ 26 cm and area ≈ 9 cm^2 was placed inside the cavity and moved with a small external magnet marked by M_P along the walls of the cavity in order to create different realizations of it. Cylindrical NiZn ferrites of diameter 33 mm and height 6 mm with saturation magnetization 2600 Oe (manufactured by SAMWHA, South Korea) were inserted into the cavity and magnetized by two external NdFeB magnets of diameter 33 mm and height 30 mm and type N42 with coercivity 11850 Oe (943 kA/m) below and above the cavity (marked by M_1 and M_2). The thereby generated homogenous magnetic field of strength $B \simeq 495$ mT induces a macroscopic magnetization of the ferrites across their cross sections. The precession of the magnetization around B with the Larmor frequency $\omega_o = \gamma B$ and gyromagnetic ratio $\gamma = 32.2$ GHz/T results in the appearance of a ferromagnetic resonance at $\nu_{fr} = 15.9$ GHz. Inducing TIV leads to different matrix elements $S_{12}(\nu) \neq S_{21}(\nu)$ of the measured scattering matrix, while for systems with preserved $\mathcal{T}$ invariance the scattering matrix is symmetric, $S_{12}(\nu) = S_{21}(\nu)$. Examples of measured spectra are presented in Fig. 1(b). The strength of TIV was controlled by varying the external magnetic field B and depends on the frequency range. It is characterized by the parameter ξ. All measurements were done in the frequency range $\nu = 6$–12 GHz for $M = 2$ scattering channels, and yielded values $\xi \simeq 0.19$–0.49. The size of ξ was determined in Ref. [41] by comparing the experimentally obtained cross-correlation coefficients

$$C_{12}^{\text{cross}} = \frac{\text{Re}[\langle S_{12}^{fl}(\nu) S_{21}^{fl*}(\nu) \rangle]}{\sqrt{\langle |(S_{12}^{fl}(\nu)|^2 \rangle \langle |(S_{21}^{fl}(\nu)|^2 \rangle}}, \quad (1)$$

where $S_{12}^{fl}(\nu) = S_{12}(\nu) - \langle S_{12}(\nu) \rangle$ denotes the fluctuating part of the scattering matrix elements, with exact analytical results. Complete TIV yields a vanishing of the cross-correlation coefficient $C_{12}^{cross} = 0$, because then $S_{12}^{fl}(\nu)$ and $S_{21}^{fl*}(\nu)$ are uncorrelated, and $C_{12}^{cross} = 1$ for $\mathcal{T}$-invariant systems. The cross-correlation coefficient is particularly small in the frequency range 7.5–9.5 GHz [41], and strongest TIV $\xi = 0.49$ is achieved for $M = 2$ open channels in the range 8–9 GHz.

The transition between GOE and GUE was verified in Ref. [41] based on an RMT approach for the fluctuation properties of the scattering matrix elements of chaotic scattering systems in the presence of absorption and partial $\mathcal{T}$-invariance violation. Here, we focus on the fluctuation properties in the resonance spectra. We restrict our analysis to $M = 2$ scattering channels as the strength ξ of TIV is largest for this case in a given frequency range. Furthermore, with increasing number of scattering channels the overlap of the resonances increases so that the identification of the eigenfrequencies from their positions becomes more cumbersome. Actually, we are not able to identify complete sequences of levels because of the strong overlap of resonances ascribed to large internal absorption in the cavity which is mainly caused by the lossy ferrites. The internal absorption γ was determined in Ref. [41] to $6 < \gamma < 15$ from the distributions of the diagonal elements of the measured scattering matrix. It is due to absorption of the electromagnetic field in the walls of the cavity and in the ferrites. The total absorption is given by $\gamma_{tot} = \gamma + \eta$ where $\eta = MT$ is the openness resulting from M open channels with transmission coefficients T. It is commonly known that ferrite is a lossy material which, near the gyromagnetic resonance, leads to an increase of the internal absorption and thus a degradation of the quality factor of the cavity. The absorption strength γ was evaluated in 1-GHz windows for $M = 2$ open channels (antennas) in Ref. [41]. With ferrites the absorption strength γ is about five times larger than without them. Nevertheless, as we presented in Ref. [29], even a fraction of $\Phi = 0.8$ identified levels suffices to classify a system with either GOE or GUE behavior according to its symmetry properties based on the analysis of missing level statistics. In the following section we address this approach and outline the procedure in detail for the present case of partially violated $\mathcal{T}$ invariance.

III. FLUCTUATION PROPERTIES OF INCOMPLETE SPECTRA IN THE PRESENCE OF PARTIAL TIV

Before comparing the spectral properties of the ensemble of microwave billiards with RMT predictions for universal quantum systems we removed system-specific properties by unfolding the resonance frequencies ν_i to mean spacing unity [60,61] with Weyl's law, $\epsilon_i = N^{Weyl}(\nu_i) = \frac{A\pi}{c_0^2} \nu_i^2 + \frac{\mathcal{L}}{2c} \nu_i +$ const, which applies to the smooth part of the integrated spectral density $N(\nu_i) = N^{Weyl}(\nu_i) + N^{fluc}(\nu_i)$.

In order to get insight into short-range correlations in the eigenfrequency spectra of the microwave billiard we analyzed the distribution $P(s)$ of the spacings between adjacent eigenvalues, $s_i = \epsilon_{i+1} - \epsilon_i$, and its cumulant $I(s)$, which has the advantage that it does not depend on the binning size of the histograms yielding $P(s)$. For the analysis of

long-range correlations we considered the variance $\Sigma^2(L) = \langle (N(L) - \langle N(L) \rangle)^2 \rangle$, of the number $N(L)$ of eigenvalues ϵ_i in an interval of length L, where $\langle N(L) \rangle = L$, and the rigidity $\Delta_3(L) = \langle \min_{a,b} \int_{e-L/2}^{e+L/2} [N(e) - a - be]^2 de \rangle$ which provides a measure for the stiffness of a spectrum. Here, $\langle \cdot \rangle$ denotes the average over an ensemble of random matrices or over the eigenvalue spectra of different realizations of the microwave billiard. Both measures may be expressed in terms of the two-point cluster function $Y_2(r)$, i.e., the rescaled two-point correlation function of two eigenvalues at a distance r, as [4]

$$\Sigma^2(L) = L - 2 \int_0^L (L - r) Y_2(r) dr, \qquad (2)$$

and

$$\Delta_3(L) = \frac{L}{15} - \frac{1}{15L^4} \int_0^L (L - r)^3 (2L^2 - 9rL - 3r^2) Y_2(r) dr. \qquad (3)$$

A further measure for long-range correlations is the power spectrum [54,62–64]

$$S(\tau) = \left\langle \left| \frac{1}{\sqrt{N}} \sum_{q=0}^{N-1} \delta_q \exp\left(-\frac{2\pi i \tau q}{N} \right) \right|^2 \right\rangle, \qquad (4)$$

with $\delta_q = \epsilon_{q+1} - \epsilon_1 - q$ denoting the deviation of the qth nearest-neighbor spacing from its mean value q. In Refs. [18,29,58] the power spectrum was investigated for the incomplete spectra of microwave networks and billiards exhibiting either GOE or GUE statistics and it was shown that $\Sigma^2(L)$ and $S(\tau)$ are particularly sensitive to missing levels. The power spectrum $S(\tau)$ only depends on the ratio $\tilde{\tau} = \tau/N$ and exhibits for $\tilde{\tau} \ll 1$ a power law dependence $\langle S(\tilde{\tau}) \rangle \propto \tilde{\tau}^{-\alpha}$ [62,63], where for regular systems $\alpha = 2$ and for chaotic ones $\alpha = 1$ independently of whether $\mathcal{T}$ invariance is preserved or not [65–69]. It can be expressed in terms of the form factor $K(\tau) = 1 - b(\tau)$ [63] where

$$b(\tau) = \int_{-\infty}^{\infty} Y_2(r) e^{-ir\tau} dr \qquad (5)$$

is the Fourier transform of the two-point cluster function.

The spectral properties are compared to analytical expressions which were obtained for the two-point cluster functions and the nearest-neighbor spacing distribution for random matrices interpolating between GOE and GUE. The matrices are given in terms of a sum

$$H_{ij} = H_{ij}^{(S)} + i\lambda H_{ij}^{(A)} \qquad (6)$$

of a real-symmetric random matrix $\hat{H}^{(S)}$ from the GOE and a real-antisymmetric one, $\hat{H}^{(A)}$. The matrix elements are uncorrelated Gaussian-distributed random numbers with zero mean and variance chosen equal to unity. The parameter ξ, which is related to λ through $\lambda = \frac{\pi \xi}{\sqrt{N}}$, determines the magnitude of $\mathcal{T}$ violation in units of the mean spacing. For $\xi = 0$, $\hat{H}$ describes chaotic systems with preserved $\mathcal{T}$ invariance, whereas for $\pi\xi/\sqrt{N} = 1$, $\hat{H}$ is a random matrix from the GUE. However, the transition from GOE to GUE already takes place for $\xi \simeq 1$ [70].

An exact analytical expression was derived for the nearest-neighbor spacing distribution in terms of a Taylor series in
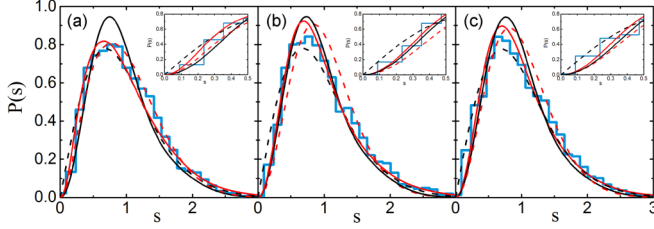
FIG. 2. Nearest-neighbor spacing distributions in the frequency ranges (a) 6.5–8 GHz, (b) 8–9 GHz, and (c) 9.2–11.5 GHz corresponding to a strength of $\mathcal{T}$-invariance violation $\xi = 0.19, 0.35$, and 0.49, respectively. The turquoise histograms show the experimental results, and the red (gray) dashed line the RMT curve for the intermediate case between GOE and GUE. The solid red (gray) line shows the result for the intermediate case with a fraction of $\Phi = 0.83, 0.81$, and 0.85 identified eigenfrequencies, respectively. The black dashed and, black solid lines show the corresponding results for GOE and GUE for these values of Φ, respectively.

Refs. [4,36]. It was shown there that it is well approximated by the Wigner-like approximation derived in Ref. [37] based on two-dimensional random matrices,

$$P(s; \lambda) = s\sqrt{\frac{2 + \lambda^2}{2}} c(\lambda)^2 \text{erf}\left(s\frac{c(\lambda)}{\lambda}\right)e^{-\frac{s^2 c(\lambda)^2}{2}}, \quad (7)$$

with $\lambda = 2\xi$,

$$c(\lambda) = \sqrt{\pi\frac{2 + \lambda^2}{4}}\left[1 - \frac{2}{\pi}\left(\tan^{-1}\left(\frac{\lambda}{\sqrt{2}}\right) - \frac{\sqrt{2}\lambda}{2 + \lambda^2}\right)\right], \quad (8)$$

and erf(x) denoting the error function. Furthermore, in Refs. [35,71] an analytical expression was derived for the two-point cluster function,

$$Y_2(L; \xi) = \det\begin{pmatrix} s(L) & -D(L; \xi) \\ -J(L; \xi) & s(L) \end{pmatrix}, \quad (9)$$

with [35,71]

$$s(L) = \frac{\sin \pi L}{\pi L}, \quad (10)$$

$$D(L; \xi) = \frac{1}{\pi}\int_0^\pi dx e^{2\xi^2 x^2} x \sin(Lx), \quad (11)$$

$$J(L; \xi) = \frac{1}{\pi}\int_\pi^\infty dx e^{-2\xi^2 x^2} \frac{\sin(Lx)}{x}. \quad (12)$$

Expressions for $\Sigma^2(L; \xi)$ and $\Delta_3(L; \xi)$ for the case of partial TIV are obtained by inserting $Y_2(L; \xi)$ into Eqs. (2), (3), and (5).

We analyzed the spectral properties of the microwave billiards in three frequency ranges, 6.5–8, 8–9, and 9.2–11.5 GHz, since the ferrite properties depend strongly on the microwave frequency and, accordingly, the degree of $\mathcal{T}$-invariance violation varies with frequency. For each of these three ranges we randomly selected 25 realizations of the cavity, yielding 110, 90, and 258 eigenfrequencies for each eigenfrequency sequence, respectively. The results for the nearest-neighbor spacing distributions, the number variance, the rigidity, and the power spectrum are shown in Figs. 2–4. Clear deviations from the corresponding theoretical curves (red dash-dotted lines) are visible.
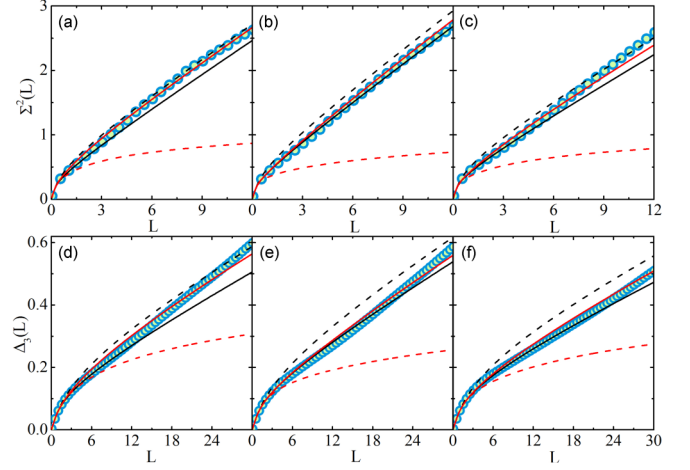

FIG. 3. Same as Fig. 2 for [(a)–(c)] the number variance and [(d)-(f)] the rigidity. The experimental results are shown as turquoise circles.

The discrepancies are attributed to missing levels. In order to derive RMT predictions for the fluctuation properties in incomplete spectra of quantum systems experiencing a partial TIV, we proceeded as in Ref. [46] on the basis of the analytical results in Eqs. (7)–(12). The derivation relies on the assumption that a fraction $1 - \Phi$ of levels are missed randomly. The nearest-neighbor spacing distribution is expressed in terms of the $(n + 1)$th-nearest-neighbor spacing distribution $P(n, s)$ with $P(0, s) = P(s)$ of the corresponding complete spectrum,

$$
\begin{aligned}
p(s) &= \sum_{n=0}^{M}(1 - \Phi)^n P\left(n; \frac{s}{\Phi}\right) \\
&\simeq \sum_{n=0}^{K-1}(1 - \Phi)^n P\left(n; \frac{s}{\Phi}\right) \\
&\quad + \sum_{n=K}^{M}\frac{(1 - \Phi)^n}{\sqrt{2\pi V^2(n)}}\exp\left(-\frac{1}{2V^2(n)}\left[\frac{s}{\Phi} - n - 1\right]^2\right),
\end{aligned}
$$

$$(13)$$

where

$$V^2(n) \simeq \Sigma^2(L = n) - \frac{1}{6}. \quad (14)$$

We chose $K = 3$ and obtained $P(n; s)$ with $n = 1, 2$ by computing the ensemble averages of the normalized next- and
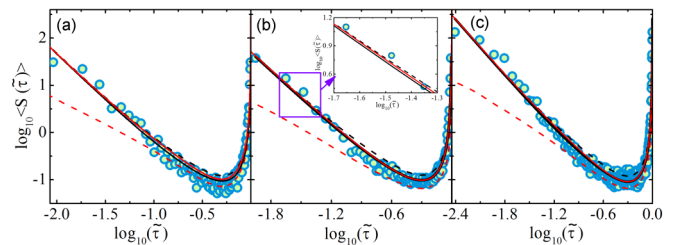

FIG. 4. Same as Fig. 2 for the power spectrum. The experimental results are shown as turquoise circles.
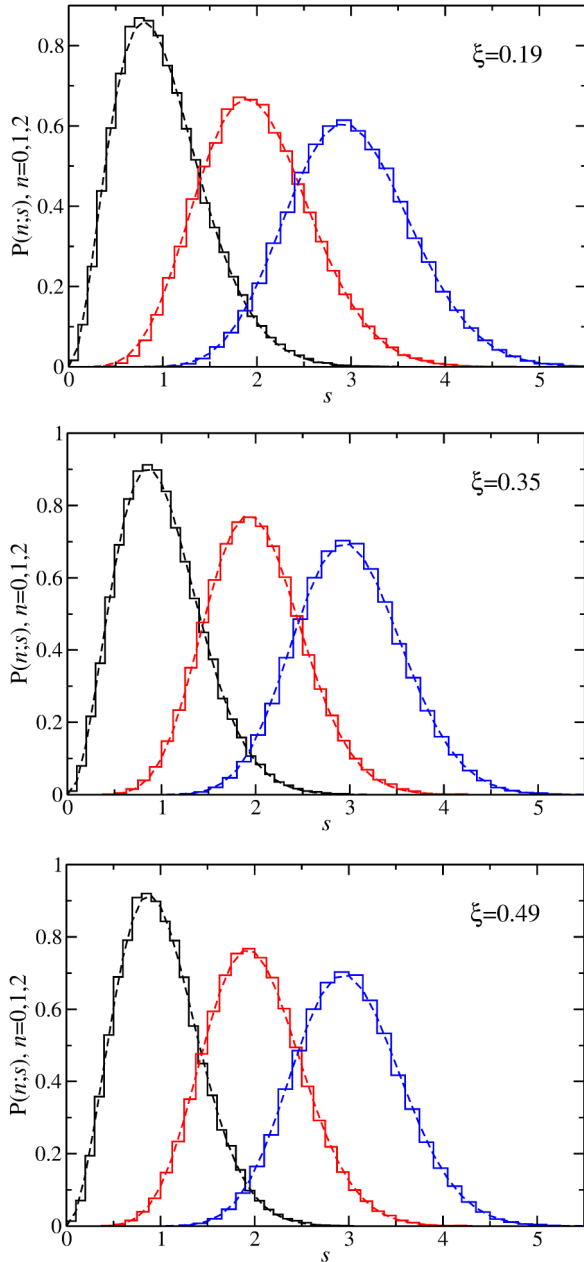
FIG. 5. Nearest-neighbor (black histogram), next-nearest-neighbor (red [gray] histogram), and second-nearest-neighbor (blue [dark gray] histogram) spacing distributions for partial $\mathcal{T}$-invariance violation where the size ξ is indicated in the panels. The dashed curves were obtained from a fit of $\tilde{P}(s) = \gamma s^{\mu} e^{-\chi s^2}$ to the histogram of corresponding color [26,49].

second-next-nearest-neighbor spacing distributions of 500 500×500 random matrices of the form of Eq. (6) and fitting $\tilde{P}(s) = \gamma s^{\mu} e^{-\chi s^2}$ to the resulting distributions, as illustrated in Fig. 5. We checked that, for larger values of n, $P(n; s)$ is well approximated by a Gaussian with variance $V^2(n)$ centered at $s = n + 1$ [72].

Since we assume that levels are missing randomly, the n-point correlation functions keep their form when a fraction $(1 - \Phi)$ of the levels is extracted and the remaining ones are

rescaled with Φ [46],

$$y_2(r) = Y_2\left(\frac{r}{\Phi}\right). \tag{15}$$

Using this feature of the two-point cluster function and Eqs. (2), (3), and (5) yields [46]

$$\sigma^2(L) = (1 - \Phi)L + \Phi^2 \Sigma^2\left(\frac{L}{\Phi}\right), \tag{16}$$

$$\delta_3(L) = (1 - \Phi)\frac{L}{15} + \Phi^2 \Delta_3\left(\frac{L}{\Phi}\right), \tag{17}$$

and

$$s(\tilde{\tau}) = \frac{\Phi}{4\pi^2}\left[\frac{K(\Phi\tilde{\tau}) - 1}{\tilde{\tau}^2} + \frac{K(\Phi(1 - \tilde{\tau})) - 1}{(1 - \tilde{\tau})^2}\right]$$
$$+ \frac{1}{4\sin^2(\pi\tilde{\tau})} - \frac{\Phi^2}{12}, \tag{18}$$

where $|\tilde{\tau}| \leqslant 1$. In that range of $\tilde{\tau}$, $b(\tilde{\tau}) = 1 - |\tilde{\tau}|$ for the GUE and $b(\tilde{\tau}) = 1 - 2|\tilde{\tau}| + |\tilde{\tau}| \ln(1 + 2|\tilde{\tau}|)$ for the GOE.

Before comparing these results to experimental ones we validated them with RMT simulations obtained for ensembles of 300 (700×700)-dimensional random matrices $\hat{H}$ as given in Eq. (6), where for illustration, we chose in Fig. 6 and in Fig. 7 for ξ and Φ the values obtained from the analysis of the experimental results. The analytical results for $\Phi = 1$ and the values of Φ given in the figures are shown as red (gray) and blue (dark gray) solid lines, respectively, and those obtained from RMT simulations as histograms and circles of corresponding color. The black solid and dashed lines show the GUE and GOE curves, respectively. The good agreement between the analytical curves and those obtained from the RMT simulations corroborates the applicability of our RMT approach to the incomplete spectra of systems with partial TIV.

The statistical measures depend on two parameters, the strength of TIV, ξ, and the fraction of identified levels, Φ. The values of ξ were determined in 1-GHz windows in Ref. [41] by fitting exact analytical expressions for the cross-correlation coefficients to the experimental results and refined by comparing the distributions of the off-diagonal elements of the measured scattering matrix and the experimentally determined enhancement factors to RMT predictions. To obtain the fraction of missing levels we used the power spectrum $\langle s(\tilde{\tau}) \rangle$ [Eq. (18)]. This measure is particularly sensitive to changes in the value of Φ [18,29,58], and above all its asymptotic behavior does not depend on the universality class. This is illustrated in the inset of Fig. 4(b). The curves for the GOE (black dashed line), the GUE (black solid line), and the intermediate case between GOE and GUE (red [gray] solid line) lie on top of each other. We inserted the resulting values of ξ into the expression in Eq. (18) and fitted then $\langle s(\tilde{\tau}) \rangle$ in the asymptotic region to the experimental curves, yielding that in the frequency ranges 6.5–8, 8–9, and 9.2–11.5 GHz, respectively, $83 \pm 3\%$, $81 \pm 3\%$, and $85 \pm 3\%$ of the resonances were identified. The errors comprise those resulting from the fitting procedure and the ensemble averaging. Note that billiard systems have the great advantage over, e.g., nuclear systems, such that an analytical expression, namely, the Weyl formula, exists for the average integrated spectral density thus providing an estimate for the value of Φ and the accuracy of the obtained value,
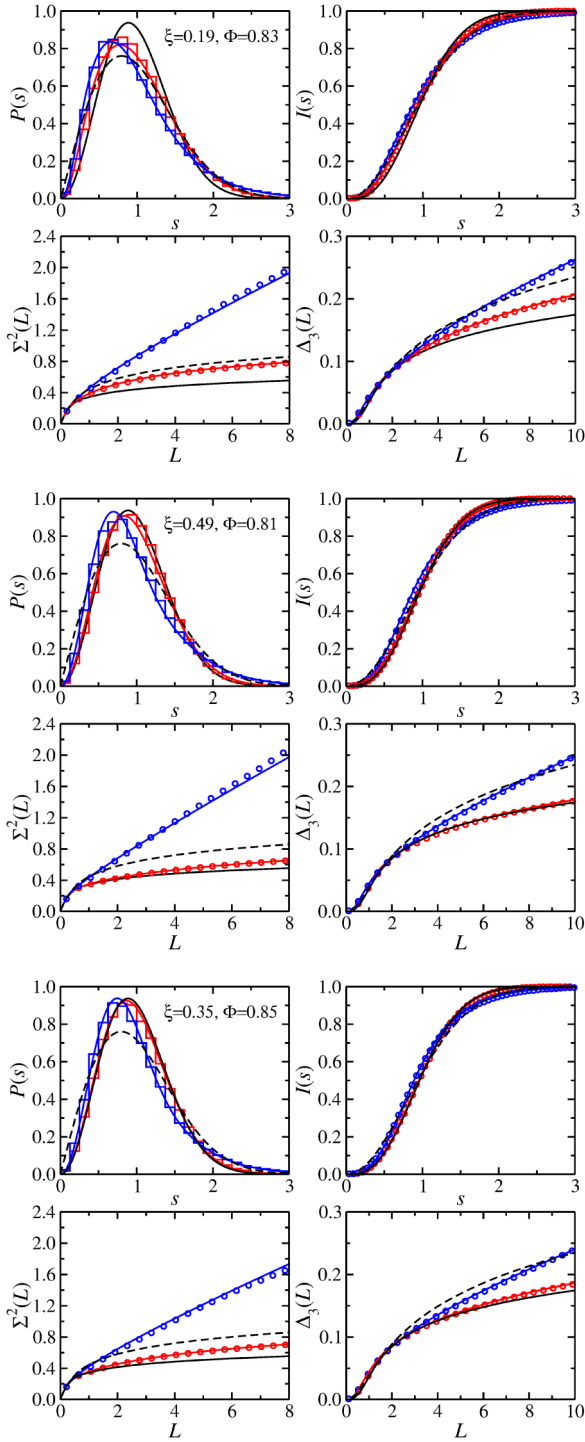
FIG. 6. Comparison of the analytical results (solid lines) for $\Phi = 1$ (red [gray]) and for the values of Φ given in the panels (blue [dark gray]) with RMT simulations (histograms and circles) which were performed based on the random matrix given in Eq. (6).
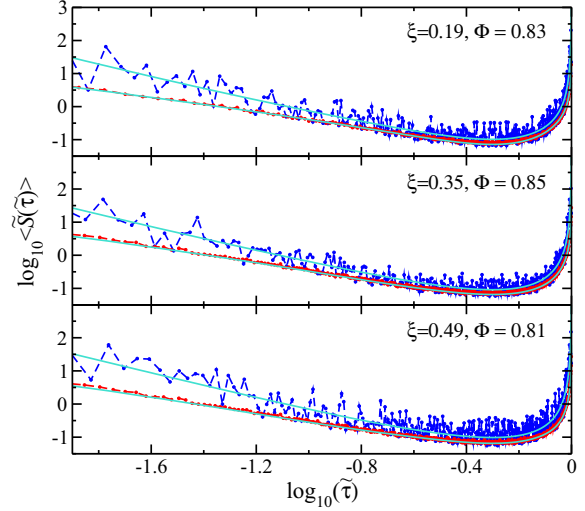

FIG. 7. Comparison of the power spectra obtained from RMT simulations based on Eq. (6) for complete spectra (red [gray] dots) and incomplete ones (blue [dark gray] dots) for partial TIV in comparison to the corresponding analytical results (turquoise solid lines) obtained from Eq. (18). The values of the fraction Φ and the strength of TIV, ξ, are given in the panels.

varying ξ by less than $\approx 20\%$ of its value, so that either an ensemble of high statistical relevance or an additional measure like the cross-correlation coefficient to obtain a statistically relevant estimate is needed. Shown are the results deduced from Eq. (16) for $\Sigma^2(L)$ for complete (black dashed line) and incomplete (black solid line) spectra at the values of ξ determined from the cross-correlation coefficient. They are compared to the curves after subtracting (turquoise [light
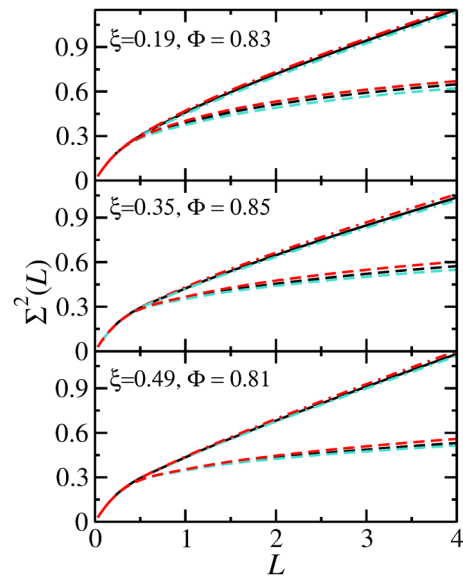

FIG. 8. Comparison of $\Sigma^2(L)$ obtained from Eq. (16) for $\Phi = 0$ (black dashed line) and incomplete (black solid line) spectra for the values of ξ and Φ given in the panels. They are compared to the corresponding analytical results with 20% added to (red [gray] lines) and subtracted (turquoise [light gray] lines) from the corresponding value of ξ.

so that a procedure like the one described in Ref. [73] is not needed. The values for Φ indeed agree with those deduced from Weyl's law within the error. The number variance $\Sigma^2(L)$ depends on the universality class and thus is used to confirm the value of ξ obtained from the cross-correlation coefficient. Yet, as illustrated in Fig. 8, $\Sigma^2(L)$ barely changes when

gray] lines) and adding (red [gray] lines) 20% of the values of ξ indicated in the panels. The rigidity $\Delta_3(L)$ is given as an integral over $\Sigma^2(L)$ and thus corresponds to a smoothing of it. It, in fact, leads to an enhancement of the differences between the curves corresponding to different values of ξ. The resulting curves are shown as red (gray) solid lines in Figs. 2–4. The agreement between the experimental and theoretical curves is good for the long-range correlation measures, whereas slight deviations are observed for the nearest-neighbor spacing distribution, as illustrated in the insets of Fig. 2. These may be attributed to the fact that eigenfrequencies may not be detected if two resonances are overlapping, that is, when they are too close to each other. This is reflected in the deviations of the experimental nearest-neighbor spacing distributions from the RMT predictions observed at small spacings. Note that the probability of a close encounter of two eigenfrequencies is small in chaotic systems, as reflected in the nearest-neighbor spacing distribution, which vanishes for zero spacing. Thus, randomness of missing levels is ensured by choosing randomly 25 different realizations of the cavity, except for small spacings. However, in experiments with microwave billiards and networks the realization of ensembles of level sequences might not be possible, so that one has to cope with randomly missing levels and also a large fraction of systematically missing ones. Such a situation indeed was encountered in an experiment with a microwave cavity [58] due to the large spectral density which led to level clustering. Yet, this can be incorporated into the appropriate random matrix model by extracting from the list of eigenvalues those with spacings to surrounding ones below a certain threshold.

IV. CONCLUSIONS

We investigated the fluctuations in the resonance frequency spectra of microwave billiards with the shape of a fully chaotic quarter bowtie microwave billiard subject to partial TIV of varying strength. The microwave billiards simulate the properties of a two-dimensional quantum billiard with $M = 2$ equivalent open channels subject to TIV. The strength of TIV is characterized by a parameter ξ and the number of missing

levels is expressed by the fraction Φ of the complete sequence of levels which could be identified. We analyze such a situation based on an RMT approach introduced in Ref. [49] to derive expressions for statistical measures of short- and long-range correlations in the spectra allowing to unambiguously assign the strength of TIV, ξ, and the fraction of missing levels, $1 - \Phi$. Since the power spectrum $\langle s(\tilde{\tau}) \rangle$ depends for small values of $\tilde{\tau} \ll 1$ only weakly on the universality class and thus on the value of ξ and, on the other hand, is sensitive to the fraction Φ of identified levels, it provides a suitable measure for the determination of Φ. Then, the number variance $\sigma^2(L)$ allows to refine or confirm the value of ξ determined from the cross-correlation coefficient. The RMT approach presented in this article reproduces very well the results obtained from RMT simulations and the experimental results for all available sets of parameters Φ, ξ, thus corroborating that it may serve as a tool to determine the extent of incompleteness of a spectrum and the value of ξ for dissipative quantum systems with classically chaotic counterpart subject to partial TIV.

The case of randomly and systematically missing levels has been addressed, e.g., in Ref. [74]. There quantum graphs and microwave networks were investigated which exhibit localized states that can be identified and extracted from the level dynamics generated by varying a parameter. This yields incomplete level sequences with systematically missing levels in addition to being due to experimental reasons randomly missing ones. In these systems the effect of the nonuniversal states on the spectral dynamics is only visible for distances below two to three mean level spacings and does not impede the determination of the fraction of missing levels and of the universality class.

[1] M. Berry, *Structural Stability in Physics* (Springer-Verlag, Berlin, 1979).

[2] G. Casati, F. Valz-Gris, and I. Guarnieri, Lett. Nuovo Cimento **28**, 279 (1980).

[3] O. Bohigas, M. J. Giannoni, and C. Schmit, Phys. Rev. Lett. **52**, 1 (1984).

[4] M. Mehta, *Random Matrices* (Elsevier Science, Amsterdam, 2004).

[5] L. Vina, M. Potemski, and W. I. Wang, Phys. Usp. **41**, 153 (1998).

[6] T. Zimmermann, H. Köppel, L. S. Cederbaum, G. Persch, and W. Demtröder, Phys. Rev. Lett. **61**, 3 (1988).

[7] L. Sirko, M. R. W. Bellermann, A. Haffmans, P. M. Koch, and D. Richards, Phys. Rev. Lett. **71**, 2895 (1993).

[8] L. Sirko and P. M. Koch, Phys. Rev. Lett. **89**, 274101 (2002).

[9] H.-J. Stöckmann and J. Stein, Phys. Rev. Lett. **64**, 2215 (1990).

[10] H.-D. Gräf, H. L. Harney, H. Lengeler, C. H. Lewenkopf, C. Rangacharyulu, A. Richter, P. Schardt, and H. A. Weidenmüller, Phys. Rev. Lett. **69**, 1296 (1992).

[11] S. Sridhar and A. Kudrolli, Phys. Rev. Lett. **72**, 2175 (1994).

[12] Y. Hlushchuk, A. Kohler, S. Bauch, L. Sirko, R. Blümel, M. Barth, and H.-J. Stöckmann, Phys. Rev. E **61**, 366 (2000).

[13] S. Hemmady, X. Zheng, E. Ott, T. M. Antonsen, and S. M. Anlage, Phys. Rev. Lett. **94**, 014102 (2005).

[14] O. Hul, N. Savytskyy, O. Tymoshchuk, S. Bauch, and L. Sirko, Phys. Rev. E **72**, 066212 (2005).

[15] B. Dietz and A. Richter, Chaos **25**, 097601 (2015).

[16] O. Hul, S. Bauch, P. Pakoński, N. Savytskyy, K. Życzkowski, and L. Sirko, Phys. Rev. E **69**, 056205 (2004).

[17] O. Hul, M. Ławniczak, S. Bauch, A. Sawicki, M. Kuś, and L. Sirko, Phys. Rev. Lett. **109**, 040402 (2012).

[18] B. Dietz, V. Yunko, M. Białous, S. Bauch, M. Ławniczak, and L. Sirko, Phys. Rev. E **95**, 052202 (2017).

[19] M. Ławniczak, J. Lipovský, and L. Sirko, Phys. Rev. Lett. **122**, 140503 (2019).

[20] K. Sacha, J. Zakrzewski, and D. Delande, Phys. Rev. Lett. **83**, 2922 (1999).

[21] L. A. Ponomarenko, F. Schedin, M. I. Katsnelson, R. Yang, E. W. Hill, K. S. Novoselov, and A. K. Geim, Science **320**, 5874 (2008).

[22] M. Aßmann, J. Thewes, and D. Fröhlich, Nat. Mat. **15**, 741 (2016).

[23] J. B. French, V. K. B. Kota, A. Pandey, and S. Tomsovic, Phys. Rev. Lett. **54**, 2313 (1985).

[24] G. E. Mitchell, A. Richter, and H. A. Weidenmüller, Rev. Mod. Phys. **82**, 2845 (2010).

[25] P. So, S. M. Anlage, E. Ott, and R. N. Oerter, Phys. Rev. Lett. **74**, 2662 (1995).

[26] U. Stoffregen, J. Stein, H.-J. Stöckmann, M. Kuś, and F. Haake, Phys. Rev. Lett. **74**, 2666 (1995).

[27] B. Dietz, T. Friedrich, H. L. Harney, M. Miski-Oglu, A. Richter, F. Schäfer, and H. A. Weidenmüller, Phys. Rev. Lett. **98**, 074103 (2007).

[28] M. Ławniczak, S. Bauch, O. Hul, and L. Sirko, Phys. Rev. E **81**, 046204 (2010).

[29] M. Białous, V. Yunko, S. Bauch, M. Ławniczak, B. Dietz, and L. Sirko, Phys. Rev. Lett. **117**, 144101 (2016).

[30] A. Rehemanjiang, M. Richter, U. Kuhl, and H.-J. Stöckmann, Phys. Rev. E **97**, 022204 (2018).

[31] M. Lawniczak and L. Sirko, Sci. Rep. **9**, 5630 (2019).

[32] J. Lu, J. Che, X. Zhang, and B. Dietz, Phys. Rev. E **102**, 022309 (2020).

[33] V. Yunko, M. Białous, and L. Sirko, Phys. Rev. E **102**, 012210 (2020).

[34] M. Ławniczak, B. van Tiggelen, and L. Sirko, Phys. Rev. E **102**, 052214 (2020).

[35] A. Pandey and P. Shukla, J. Phys. A **24**, 3907 (1991).

[36] B. Dietz, Ph.D. thesis, Fachbereich Physik der Universität-Gesamthochschule Essen, 1991.

[37] G. Lenz and K. Życzkowski, J. Phys. A **25**, 5539 (1992).

[38] S. Schierenberg, F. Bruckmann, and T. Wettig, Phys. Rev. E **85**, 061130 (2012).

[39] B. Dietz, T. Friedrich, H. L. Harney, M. Miski-Oglu, A. Richter, F. Schäfer, J. Verbaarschot, and H. A. Weidenmüller, Phys. Rev. Lett. **103**, 064101 (2009).

[40] B. Dietz, T. Klaus, M. Miski-Oglu, A. Richter, and M. Wunderle, Phys. Rev. Lett. **123**, 174101 (2019).

[41] M. Białous, B. Dietz, and L. Sirko, Phys. Rev. E **102**, 042206 (2020).

[42] B. Dietz, H. L. Harney, O. N. Kirillov, M. Miski-Oglu, A. Richter, and F. Schäfer, Phys. Rev. Lett. **106**, 150403 (2011).

[43] S. Bittner, B. Dietz, U. Günther, H. L. Harney, M. Miski-Oglu, A. Richter, and F. Schäfer, Phys. Rev. Lett. **108**, 024101 (2012).

[44] B. Dietz, T. Guhr, B. Gutkin, M. Miski-Oglu, and A. Richter, Phys. Rev. E **90**, 022903 (2014).

[45] B. Dietz, T. Klaus, M. Miski-Oglu, A. Richter, M. Wunderle, and C. Bouazza, Phys. Rev. Lett. **116**, 023901 (2016).

[46] O. Bohigas and M. P. Pato, Phys. Lett. B **595**, 171 (2004).

[47] U. Agvaanluvsan, G. E. Mitchell, J. F. Schriner, Jr., and M. P. Pato, Nucl. Instrum. Methods Phys. Res. A **498**, 459 (2003).

[48] U. Agvaanluvsan, G. E. Mitchell, J. F. Shriner, and M. Pato, Phys. Rev. C **67**, 064608 (2003).

[49] O. Bohigas and M. P. Pato, Phys. Rev. E **74**, 036212 (2006).

[50] H. I. Liou, H. S. Camarda, and F. Rahn, Phys. Rev. C **5**, 1002 (1972).

[51] T. A. Brody, J. Flores, J. B. French, P. A. Mello, A. Pandey, and S. S. M. Wong, Rev. Mod. Phys. **53**, 385 (1981).

[52] J. Enders, T. Guhr, N. Huxel, P. von Neumann-Cosel, C. Rangacharyulu, and A. Richter, Phys. Lett. B **486**, 273 (2000).

[53] J. Enders, T. Guhr, A. Heine, P. von Neumann-Cosel, V. Ponomarev, A. Richter, and J. Wambach, Nucl. Phys. A **741**, 3 (2004).

[54] R. Molina, J. Retamosa, L. Muñoz, A. Relaño, and E. Faleiro, Phys. Lett. B **644**, 25 (2007).

[55] A. Frisch, M. Mark, K. Aikawa, F. Ferlaino, J. L. Bohn, C. Makrides, A. Petrov, and S. Kotochigova, Nature (London) **507**, 474 (2014).

[56] J. Mur-Petit and R. A. Molina, Phys. Rev. E **92**, 042906 (2015).

[57] M. Białous, V. Yunko, S. Bauch, M. Ławniczak, B. Dietz, and L. Sirko, Phys. Rev. E **94**, 042211 (2016).

[58] M. Ławniczak, M. Białous, V. Yunko, S. Bauch, and L. Sirko, Phys. Rev. E **98**, 012206 (2018).

[59] M. Białous, B. Dietz, and L. Sirko, Phys. Rev. E **100**, 012210 (2019).

[60] H.-J. Stöckmann, *Quantum Chaos: An Introduction* (Cambridge University Press, Cambridge, UK, 2000).

[61] F. Haake, *Quantum Signatures of Chaos* (Springer-Verlag, Heidelberg, 2001).

[62] A. Relaño, J. M. G. Gómez, R. A. Molina, J. Retamosa, and E. Faleiro, Phys. Rev. Lett. **89**, 244102 (2002).

[63] E. Faleiro, J. M. G. Gómez, R. A. Molina, L. Muñoz, A. Relaño, and J. Retamosa, Phys. Rev. Lett. **93**, 244101 (2004).

[64] R. Riser, V. A. Osipov, and E. Kanzieper, Phys. Rev. Lett. **118**, 204101 (2017).

[65] J. M. G. Gómez, A. Relaño, J. Retamosa, E. Faleiro, L. Salasnich, M. Vraničar, and M. Robnik, Phys. Rev. Lett. **94**, 084101 (2005).

[66] L. Salasnich, Phys. Rev. E **71**, 047202 (2005).

[67] M. S. Santhanam and J. N. Bandyopadhyay, Phys. Rev. Lett. **95**, 114101 (2005).

[68] A. Relaño, Phys. Rev. Lett. **100**, 224101 (2008).

[69] E. Faleiro, U. Kuhl, R. Molina, L. Muñoz, A. Relaño, and J. Retamosa, Phys. Lett. A **358**, 251 (2006).

[70] B. Dietz, T. Friedrich, H. L. Harney, M. Miski-Oglu, A. Richter, F. Schäfer, and H. A. Weidenmüller, Phys. Rev. E **81**, 036205 (2010).

[71] O. Bohigas, M.-J. Giannoni, A. M. O. de Almeidaz, and C. Schmit, Nonlinearity **8**, 203 (1995).

[72] O. Bohigas, P. Leboeuf, and M. Sánchez, Physica D **131**, 186 (1999).

[73] I. Casal, L. Muñoz, and R. A. Molina, Eur. Phys. J. Plus **136**, 263 (2021).

[74] J. Che, J. Lu, X. Zhang, B. Dietz, and G. Chai, Phys. Rev. E **103**, 042212 (2021).